Cavity dumping using a microscopic Fano laser

Dong, Gaoneng; Liang, Shih Lun; Sakanas, Aurimas; Semenova, Elizaveta; Yvind, Kresten; Mørk, Jesper; Yu, Yi

Published in:
Optica

Link to article, DOI:
10.1364/OPTICA.476758

Publication date:
2023

Document Version
Publisher's PDF, also known as Version of record

OPTICA

Cavity dumping using a microscopic Fano laser

Gaoneng Dong,[1,2] Shih Lun Liang,[1,2] Aurimas Sakanas,[1,2] Elizaveta Semenova,[1,2] Kresten Yvind,[1,2] Jesper Mørk,[1,2,3] and Yi Yu[1,2,*]

[1]DTU Electro, Technical University of Denmark, Lyngby, Denmark
[2]NanoPhoton—Center for Nanophotonics, Technical University of Denmark, Lyngby, Denmark
[3]e-mail: jesm@dtu.dk
*Corresponding author: yiyu@dtu.dk

Received 27 September 2022; revised 22 December 2022; accepted 27 December 2022; published 3 February 2023

A microlaser with low energy consumption and high speed is crucial for on-chip photonic networks. Presently, the modulation of microlasers is based on modulating the gain of the laser, which implies a trade-off between the output peak power and modulation energy. Also, the temporal width of the output pulse is restricted by the carrier relaxation time. These limitations can be overcome by modulating, instead, the loss of the laser by the scheme of cavity dumping, which is ideal for intense and ultrashort pulse generation. However, the miniaturization of cavity-dumped lasers has been a long-standing challenge, and no microscopic cavity-dumped lasers have yet been realized. Here, we demonstrate an ultra-small cavity-dumped microscopic laser based on an optical Fano resonance, which generates optical pulses with peak power more than one order of magnitude higher than the corresponding conventional gain-modulated laser. This demonstration paves the way for realizing microscopic lasers for low-power chip-scale applications.

https://doi.org/10.1364/OPTICA.476758

1. INTRODUCTION

On-chip optical interconnects [1] have the potential to overcome the limits on bandwidth and power consumption in traditional electrical interconnects [2]. The transmitter in an on-chip optical network needs to meet several demanding requirements, i.e., sufficient peak power, high speed, low energy consumption, and ultra-small footprint. One well-known transmitter configuration integrates external modulators [3,4] with continuous-wave (CW) microlasers [5,6]. Another simpler one is the directly modulated microlaser. The latter generally has much lower power consumption, smaller size, and lower cost, and has been widely investigated [7–14]. However, these microlasers are all based on modulating the gain of the laser, implying a trade-off between the output peak power and modulation energy [14]. In addition, the modulation bandwidth is inherently limited by the relaxation oscillation frequency.

One way to overcome these obstacles is to use the scheme of cavity dumping, where the output power is modulated via the cavity loss rather than the gain of the laser. The cavity-dumped laser was first demonstrated more than 50 years ago [15], and has been applied in numerous configurations to generate high-peak-power pulses with pulse durations from nanoseconds [16–19] to femtoseconds (combined with mode-locking techniques) [20–23]. However, these configurations are traditionally based on large and complicated multi-element systems with meter-sized cavity lengths. Recently, several integrated lasers exploiting reflectivity modulation were demonstrated [24–27]. Tessler *et al*. reported a wide-band amplitude modulation edge-emitting laser [27]; Shchukin *et al*. demonstrated a large-bandwidth vertical-cavity surface-emitting laser (VCSEL) [26], in both cases by tuning the stopband edge of distributed Bragg reflectors (DBRs); Dong *et al*. reported reflectivity-modulated lasers by employing a composite mirror [24,25]. These systems, however, still have relatively large footprints, and are complex and energy consuming.

Here, we demonstrate a microscopic cavity-dumped laser with a mirror based on optical Fano resonance [28,29]. The rich physics of Fano resonances has been studied in numerous photonic and plasmonic nanostructures [30,31]. In particular, by replacing one laser mirror with a narrowband mirror, the so-called Fano laser has been demonstrated [32,33], showing several important features, including suppression of feedback-induced instabilities [34], self-pulsing [32], and orders-of-magnitude reduction of the laser linewidth [35]. In this work, we experimentally and theoretically demonstrate that the output power of a Fano laser can be efficiently modulated via the nanocavity to perform cavity dumping, leading to the generation of optical pulses with peak power more than one order of magnitude higher than that of an equivalent gain-modulated laser.

2. CONCEPT, SCHEMATIC, AND PRINCIPLE

The conventional way of modulating a laser is via the gain, cf. Fig. 1(a) (here, we refer to the laser bias as the pumping source). Such a modulation scheme typically cannot generate high-peak-power pulses since the maximum output power of the laser is limited by the modulation depth $\Delta R/R$, where R is the initial pumping rate, and ΔR is the change. Thus, if the initial constant

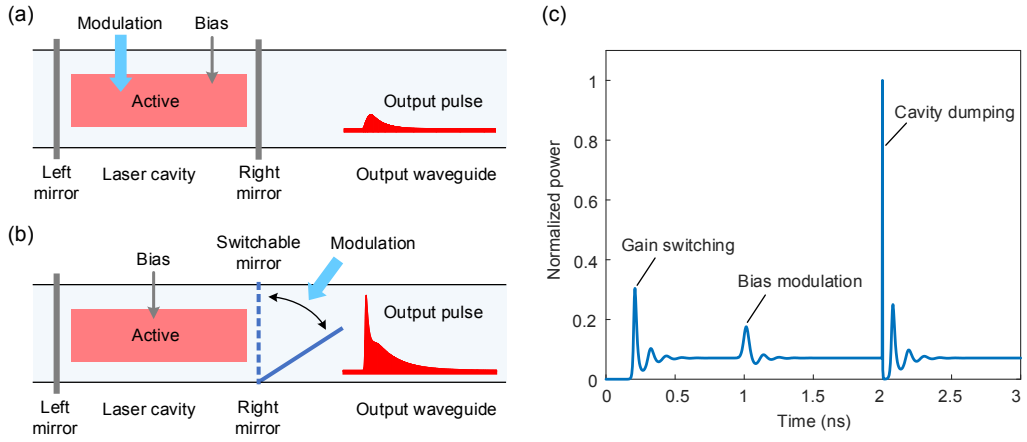

Fig. 1. (a) Concept of a conventional gain-modulated laser. An external modulation changes the gain of the active region in the laser cavity, resulting in the generation of an optical pulse. (b) Concept of a cavity-dumped laser. The reflectivity of one of its mirrors is changed by external modulation, releasing the optical energy in the laser cavity within a short time and thereby generating an optical pulse with high peak power in the output waveguide. (c) Example of the computed dynamics of the output power (normalized) for cavity dumping, bias modulation, and gain switching. The spontaneous emission factors β_{sp} and maximum amplitude change of the reflection coefficient Δr_R are 0.001 and 0.1, respectively.

bias is above the laser threshold (called bias modulation), the peak modulated power scales as $P_{b,peak} = P_s + \eta_p(\Delta R/R)P_s$, where P_s is the initial output power at steady state, and η_p is a coefficient smaller than one (Supplement 1 A.1). Instead, the cavity-dumped laser modulates the output signal via one of its mirrors, which acts as a switchable "gate." For example, by applying an external optical pulse, the right mirror "opens" [Fig. 1(b)], and a large number of photons initially stored in the laser cavity can thus be dumped within a short time, generating a high-peak-power optical pulse at the output. In this case, the maximum output power of the pulse, achieved if the "gate" is opened instantaneously, is (Supplement 1 A.1)

$$P_{d,peak} = P_s + \frac{\Delta r_R\,(2r_R - \Delta r_R)}{t_R^2} P_s, \tag{1}$$

where r_R (t_R) is the reflection (transmission) coefficient (assumed to be real) of the right mirror at steady state, and Δr_R is the maximum amplitude change of the reflection coefficient. Since usually $r_R \to 1$ and $t_R^2 \ll 1$, $P_{d,peak}$ can be much larger than $P_{b,peak}$, cf. Fig. 1(c). It should be noted that by modulating the gain and keeping the initial constant bias below the laser threshold, one can also generate optical pulses, similar to the bias-modulation scheme (called gain switching [36]). However, the maximum power $P_{g,peak}$ is still limited by the pumping rate, and much lower than $P_{d,peak}$, cf. Fig. 1(c). For higher spontaneous emission factors, β_{sp}, which is the case for microscopic lasers, and a larger maximum amplitude change of the reflection coefficient, Δr_R, the advantage of the cavity dumping scheme becomes more significant in terms of peak power (Supplement 1 A.1). Additionally, the time duration of the cavity-dumped output pulse, unless limited by the switching time of the laser mirror, will be determined by the round trip time of the laser cavity. This round trip time can be very short (femtoseconds for microscopic lasers, Supplement 1 A.1), orders of magnitude faster than the conventional gain-modulated scheme where the pulse duration is limited by the carrier relaxation time (typically on the order of several picoseconds even for high pumping rates).

Here, we realize a microscopic cavity-dumped laser that exploits an optical Fano resonance. The laser is based on a photonic crystal (PhC) membrane structure on silicon composed of a line-defect waveguide (WG) and two qualitatively different mirrors [Fig. 2(a)], with an effective footprint of only $12.5 \times 6\ \mu m^2$. The left mirror is a conventional broadband mirror formed by simply terminating the WG with holes, while the right switchable mirror is based on the Fano resonance originating from the interaction between the continuum of WG modes and the discrete mode of a side-coupled nanocavity. Specifically, the discrete mode is the second-order mode of an L7 nanocavity formed by omitting seven air holes. Due to the Fano destructive interference at the output of the right mirror, wavelengths close to the resonance of the nanocavity will be reflected with a near-unity reflection coefficient [Fig. 2(b)]. If the total nanocavity decay rate is dominated by the coupling rate γ_c between the nanocavity and the WG, rather than by the intrinsic decay rate γ_v of the nanocavity, the transmissivity ($\gamma_v/(\gamma_v + \gamma_c)$) at the nanocavity resonance will be much smaller than the out-of-plane scattering of the nanocavity ($\sqrt{\gamma_c\gamma_v}/(\gamma_v + \gamma_c)$). This feature of the Fano mirror is favorable for generating optical pulses with high contrast in the output WG (through-port). Similar to our recent demonstration of an ultracoherent Fano laser [35], we use a buried-heterostructure (BH) region [12] containing a single InGaAsP/InAlGaAs quantum well [Fig. 3(a)] to confine the active material to the laser cavity while leaving the remaining area passive. Here, we refer to the laser cavity as the region between the left mirror and the Fano mirror to separate it from the nanocavity. Details of the design and fabrication can be found in Ref. [35].

The Fano laser is optically pumped by a CW laser via a broadband grating coupler [37] located at the right end of the WG [Fig. 2(a)]. The detailed modulation principle is illustrated in Fig. 2(c). At steady state, the lasing wavelength is aligned to the peak reflectivity of the narrowband Fano mirror so the optical field is well confined in the laser cavity and the nanocavity [see the upper panel of Fig. 2(d)]. An optical pulse is injected from the top and is coupled into the third-order mode of the nanocavity. This mode, in contrast to the second-order mode of the nanocavity, is spatially concentrated in the region of the nanocavity, i.e., it hardly couples to the WG mode [see the bottom panel of Fig. 2(d)]. Such a strong field localization not only causes an effective local index change

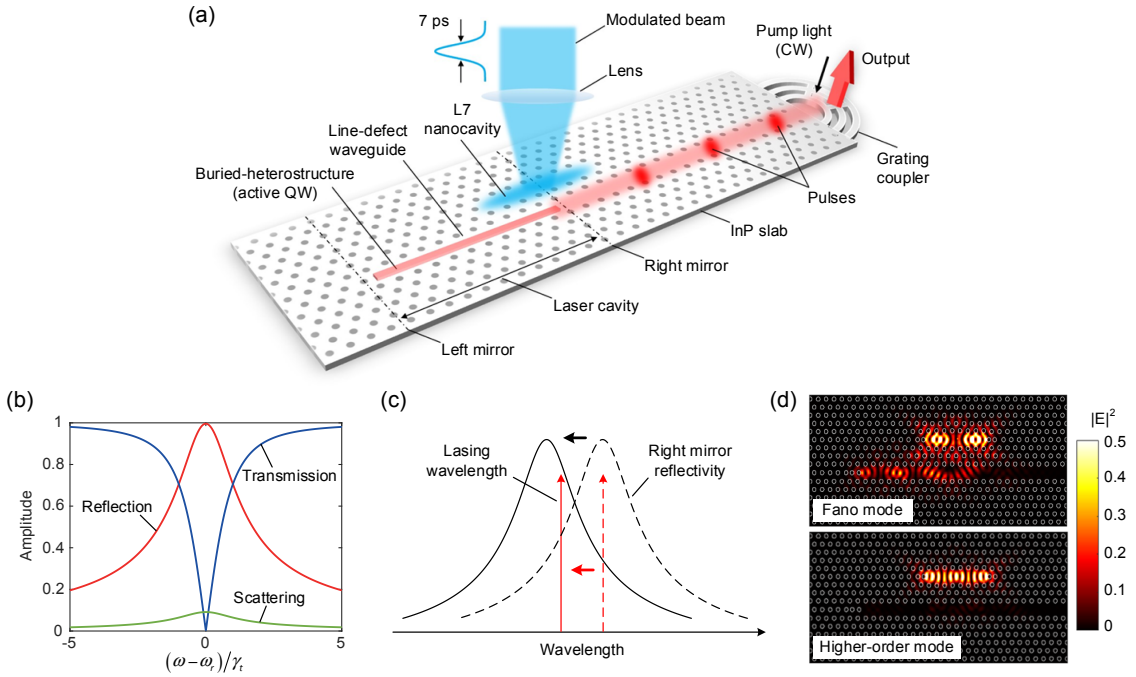

Fig. 2. Schematic and principle of cavity-dumped Fano laser. (a) Schematic of the optically modulated cavity-dumped Fano laser based on a Fano mirror formed by coupling a photonic crystal waveguide with a side-coupled nanocavity. (b) Example of calculated amplitude of reflection coefficient (red line), transmission coefficient (blue line), and out-of-plane scattering (green line) of a Fano mirror. The intrinsic Q-factor Q_v and coupling Q-factor Q_c of the nanocavity are 120,000 and 500, respectively. (c) Principle of the switchable (Fano) mirror. With the blueshift of the nanocavity resonance, the lasing wavelength (solid vertical red arrow) will partially track the peak of the reflection spectrum (solid black curve), but the effective detuning will increase, leading to a reduction in reflectivity. (d) Calculated (normalized) optical intensity profiles ($|E|^2$) of the two relevant optical modes, both shown in the center plane of the PhC membrane. The colorbar is saturated at 0.5 for clarity. The upper panel shows the Fano mode (corresponding to the second-order mode of the L7 nanocavity), in which the laser oscillates, and the lower panel shows a higher-order mode (corresponding to the third-order mode of the L7 nanocavity), which is mainly concentrated in the L7 nanocavity and used for modulating the nanocavity and thereby the right mirror.

through optical nonlinearities that quickly blueshift the resonant frequency of the nanocavity, but also ensure that the nanocavity rather than the entire laser gets modulated. During the resonance shift, the lasing wavelength will partially track the nanocavity resonance, but with an increasing effective detuning [33], leading to a reduction (increase) in reflectivity (transmissivity) of the laser mirror [Fig. 2(c)]. Thus, the photons stored in the laser cavity are coupled out via the through-port.

3. DEMONSTRATION OF CAVITY DUMPING

Under constant pumping, the Fano laser oscillates in a single mode, as observed in our previous works [32,35]. Figure 3(b) depicts the output peak power versus pump power, showing a clear transition to lasing at a threshold pump power of −5 dBm. The measured maximum output power is about −50 dBm. For comparison, a PhC line-defect laser, which can effectively be considered as a Fabry–Perot (FP) laser, is also characterized [Fig. 3(c)]. The FP

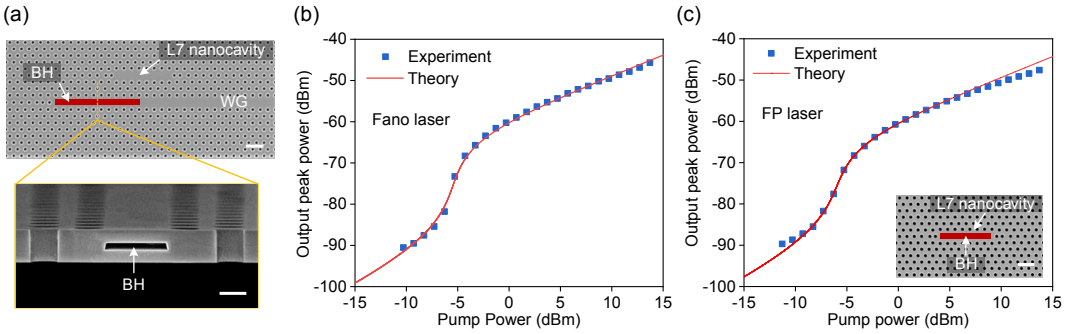

Fig. 3. Device and statistic characteristics. (a) Scanning electron microscope (SEM) image of a fabricated Fano laser (upper panel) based on an InP PhC membrane structure embedded with a buried heterostructure (BH, red rectangle) gain region composed of a single quantum well. The side-coupled L7 nanocavity is passive. Scale bar: 1 μm. The inset (lower panel) is the SEM image of the cross section of a fabricated Fano laser showing the active waveguide containing a BH. Scale bar: 200 nm. (b), (c) Collected output peak power of the laser spectra (OSA resolution: 0.1 nm) versus pump power for the Fano laser (b) and the FP laser (c). The pump power refers to the value after the microscope's objective lens. The blue squares are experimental data, and the red lines are theoretical results based on rate equations with fitted parameters. The inset in (c) shows the SEM image of the FP laser with a BH (red rectangle) embedded only within the L7 nanocavity. Scale bar: 1 μm.

laser is identical to the side-coupled nanocavity used in the Fano laser except for embedding an active BH into the nanocavity. The FP laser is vertically pumped with the same light source as the Fano laser, and the emission is collected vertically (Supplement 1 B.1 and B.2 detail the static and dynamic measurement setups). Although the pumping and collection schemes differ, the two lasers show very similar characteristics in terms of laser threshold and collected output power.

To verify the observation of cavity dumping, we measure the dynamics of the output signal of the Fano laser coupled via the through-port (emission from the grating coupler) and the cross-port (emission from the nanocavity). We also characterize the dynamics of the FP laser by aligning the modulating pulse to the third-order mode of the L7 nanocavity, where the pump and modulation powers are the same as for the Fano laser.

The output waveforms of the Fano laser [Fig. 4(a), after subtracting the noise of the erbium- doped fiber amplifier (EDFA) (Supplement 1 D)] differ qualitatively between the through- and cross-ports. The through-port signal exhibits a high-contrast "peak," while a "dip" appears in the cross-port signal [Fig. 4(a)]. The cross-port signal directly reflects the energy stored in the laser cavity, which follows an opposite time evolution as the through-port signal that reflects the cavity-dumped energy. This is a typical feature of cavity-dumped lasers [16,18,19]. In contrast, the output signal from the FP laser evolves in the same way as the injected signal, reflecting the conventional gain-modulation scheme.

The measured spectra of the Fano laser are asymmetric with an enhanced blue component seen in both through- and cross-port signals [Fig. 4(b)], which is in accordance with the modulation mechanism of the Fano mirror [Fig. 2(c)]. The spectral broadening is much larger for the through-port signal than for the cross-port signal, which is consistent with their waveforms [Fig. 4(a)]. The measurements can be well fitted by our numerical simulations (Supplement 1 A.2 and A.3), cf. Figs. 4(c) and 4(d), showing that the corresponding maximum amplitude change of the reflection coefficient of the Fano mirror is smaller than 0.1 [see the red curve in Fig. 4(e)]. In addition, the loss of the Fano laser is varying in time and is governed by the mirror loss, which increases rapidly after the arrival of the modulating pulse [see the upper panel of Fig. 4(f)] due to the resonance shift of the nanocavity. The Fano laser switches from the initial "ON" state to the "OFF" state as the loss suddenly exceeds the gain. In contrast, the loss of the FP laser remains constant [see the lower panel of Fig. 4(f)], in accordance with the gain modulation due to linear absorption of the modulated light in the third-order mode of the L7 nanocavity (Supplement 1 C.3). Although the nonlinear absorption in the nanocavity (including two-photon absorption and free-carrier absorption) can also lead to the transmissivity increase of the Fano mirror, it is unfavorable for high-power pulse generation, causing a reduction in peak power by 30% according to simulations. It should be emphasized that for the Fano laser, the measured waveforms are limited by the time resolution of the oscilloscope, which is not the case for the FP laser due to the long duration of its output pulse. The actual pulse peak power of the Fano laser is 50% higher than the measured value [see the inset in Fig. 4(c)]. Although cavity dumping is an effective approach to generate ultrashort pulses, in our case, the pulse suffers from a relatively long tail, which is due to the long lifetime of free carriers generated in the nanocavity [38]. In addition, following the cavity dumping, when the gain eventually exceeds the loss as the Fano resonance shifts back [see the

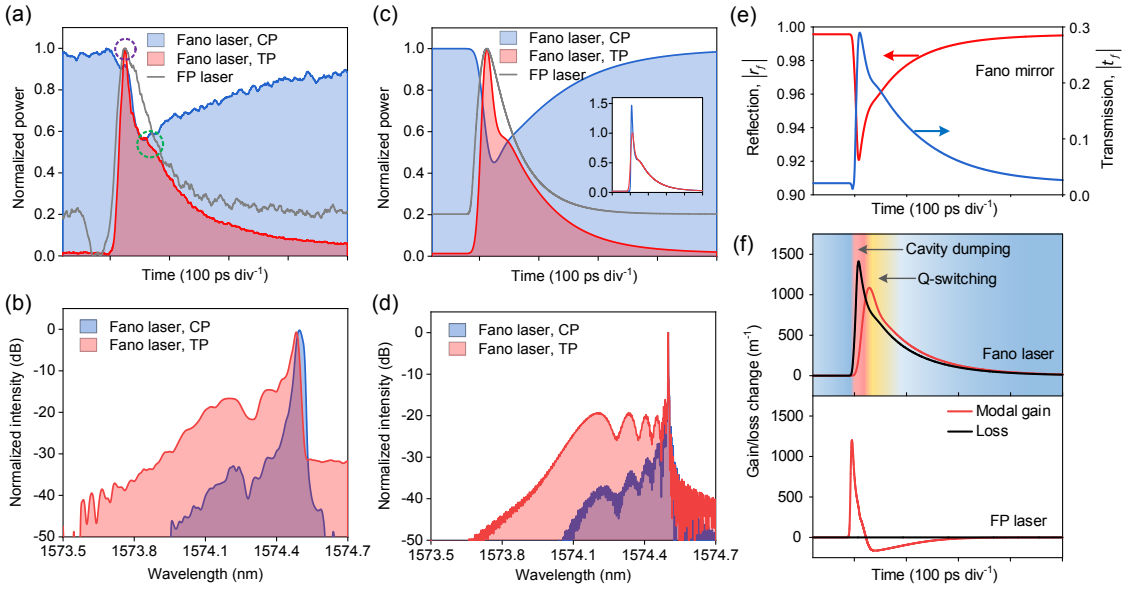

Fig. 4. Demonstration of cavity dumping in a Fano laser. (a), (b) Measured (normalized) waveforms (a) and spectra (b) of the through-port (TP) and cross-port (CP) signals of the Fano laser. The main peak of the TP signal in (a) (marked by the purple dashed circle) is generated by cavity dumping, while the following kink (marked by the green dashed circle) is due to cavity Q-switching. The gray curve in (a) represents the measured (normalized) waveform of the FP laser. The pumping rate and average modulation power are 79 P_{th} and 1.26 mW, respectively, for both lasers. (c), (d) Calculated (normalized) waveforms (c) and spectra (d) of the TP and CP signals of the cavity-dumped Fano laser. The gray curve in (c) represents the calculated (normalized) waveform of the FP laser. The pumping rate and average modulation power are 79 P_{th} and 1.26 mW, respectively, for both lasers. Note that the calculated waveforms have been convoluted with the oscilloscope pulse response (16.5 ps). Inset in (c): calculated waveforms from the TP of the Fano laser with (red curve) and without (blue curve) convolution with the oscilloscope pulse response. They are both normalized by the peak of the red curve. (e) Calculated time evolution of the amplitude of the reflection coefficient (r_f) and transmission coefficient (t_f) of the Fano mirror during modulation. (f) Calculated time dependence of the gain (red curve) and loss (black curve) change for the Fano laser (upper panel) and the FP laser (lower panel) during modulation. In the upper panel, the pink (yellow) shaded area refers to the cavity dumping (Q-switching) region of the Fano laser.

upper panel of Fig. 4(f)], the laser switches from the "OFF" state back to the "ON" state, releasing a "secondary pulse" due to cavity Q-switching [33], thus adding a kink and elongating the tail of the output waveform, cf. Figs. 4(a) and 4(c). Our theoretical model predicts that for larger modulation power, the "primary" and "secondary" pulses can be well separated in time, which narrows the time width of the main pulse (Supplement 1 C.2). This indicates that a short pulse may still be generated even in the presence of a long carrier lifetime.

4. DYNAMICS CHARACTERISTICS

Next, we compare the dynamics of the Fano laser and FP laser in dependence of the modulation and pump powers. The power value is measured at the final detector, and the estimated ratio of the coupling efficiencies (from the output of the laser mirror to the detector) of the Fano and FP lasers is about 2–6. The peak power of the Fano laser increases efficiently with both the modulation power [Fig. 5(a)] and pump power [Fig. 5(d)], which is not the case for the FP laser [Figs. 5(b) and 5(e)]. This is also reflected in their corresponding spectra (Supplement 1 C.1), and in accordance with our simulations (Supplement 1 C.2). A direct comparison is provided in Fig. 5(c) (varying the average modulation power, while keeping the pump power constant) and Fig. 5(f) (varying the pump power, while keeping the modulation power constant). The peak power of the output pulse from the Fano laser is more than one order of magnitude higher than the FP laser (11–33 times when normalized by the coupling efficiency). According to our simulations, a further improvement by more than two orders of magnitude should be achievable for higher modulation powers [Fig. 5(c)], which are, however, not attainable in our experimental setup. This reflects the intrinsic advantage of the cavity-dumping scheme enabled by the Fano laser compared to the gain-modulation scheme, cf. earlier discussion of the trade-off between the output peak power and modulating pulse energy (Supplement 1 A.1 and A.3). For optical pumping, the ratio of the output peak power with respect to the average input modulation power, P_o^p/P_i^p, increases monotonically with P_i^p for the Fano laser [Fig. 5(c), Supplement 1 A.2], while the peak power of the FP laser saturates [Fig. 5(c)], which is due to carrier density saturation under optical modulation (Supplement 1 A.3). Although such a saturation effect is expected to be eliminated under electrical modulation, which is beyond the scope of this work and requires further investigations, our preliminary simulations show that compared to the FP laser, the pulse peak power of the Fano laser is still much higher and increases much faster with the modulation/pump power, due to the nature of cavity dumping.

5. DISCUSSION AND CONCLUSION

Theoretical fits to the experimental results suggest that the initial lasing wavelength of the Fano laser is slightly detuned with respect to the peak of the Fano mirror reflectivity due to fabrication imperfections, which degrades the quality of the output pulse. This can be alleviated by using a microheater [39] to tune the nanocavity resonance or the phase delay in the WG. The slow carrier lifetime in the nanocavity sets a limit on the pulse duration and thus the modulation speed of the Fano laser. This problem

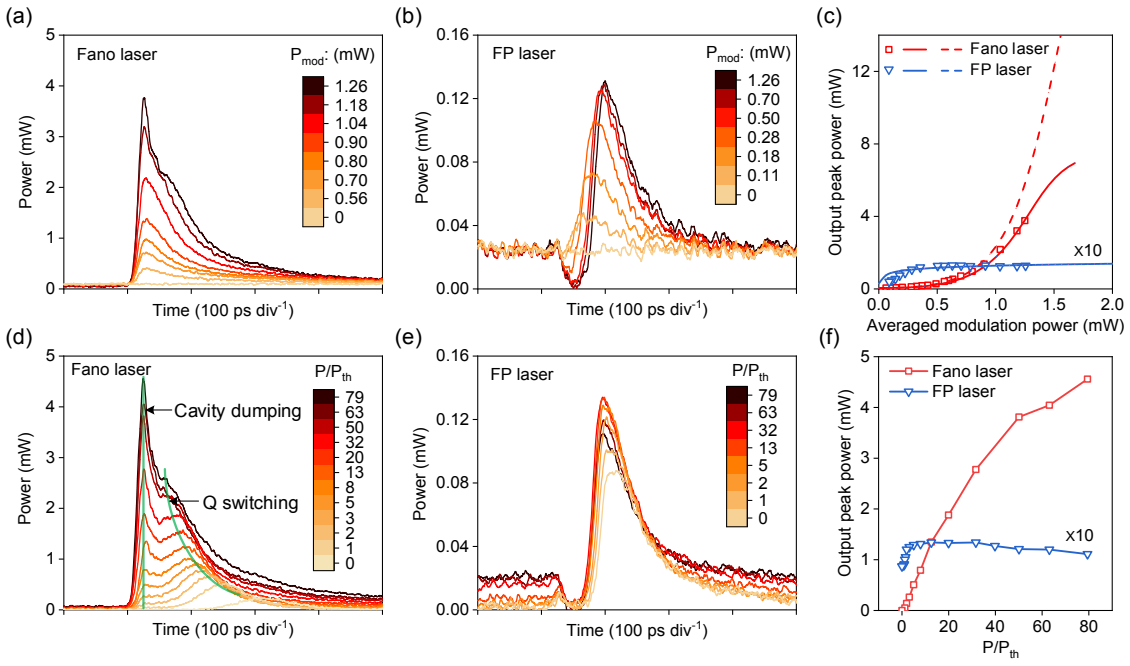

Fig. 5. Dynamic characteristics of cavity-dumped Fano laser. (a), (b) Measured waveforms of the through-port signal of the Fano laser (a) and the signal emitted from the top of the FP laser (b) for different values of modulation power. The pumping rate is 63 P_{th} for both lasers. The average modulation power refers to the value measured after the microscope objective lens. (c) Output peak power versus average modulation power. The symbols are the measured results, while the solid (dashed) line is the calculated result after (before) the convolution with the oscilloscope pulse response. The solid and dashed lines overlap for the FP laser. The calculated output peak power is amplified by 28 dB for both lasers to match the experimental results (with the EDFA amplification in front of the oscilloscope). (d), (e) Measured waveforms of the through-port signal of the Fano laser (d) and the signal emitted from the top of the FP laser (e) with varied pump power. The average modulation power is fixed at 1.26 mW for both lasers. In (d), the left green line indicates the peak associated with cavity dumping, and the right green curve indicates the peak associated with cavity Q-switching. (f) Output peak power [refers to the narrow front peak in (d)] versus pump power. In (c) and (f), the output peak power of the FP laser is multiplied by another factor of 10 to make it clearer for comparison.

might be overcome by employing carrier sweeping [40], or replacing the nanocavity material with one where instantaneous optical Kerr [41] or Pockels electro-optic [42] effects dominate. The frequency chirping imposed on the out-coupled pulse, appearing to be unavoidable for Fano laser modulation, is not a problem for on-chip applications because the optical interconnect distances are so short that the effects of the pulse dispersion are negligible. According to our simulations, although the absorbed energy for modulation (∼16 fJ/pulse) is currently larger than the generated pulse energy (∼0.85 fJ/pulse), the modulation energy can be significantly decreased by increasing the Q-factor or reducing the mode volume of the nanocavity, which can lead to a higher localization of the nanocavity field and thus stronger optical nonlinearities, as verified by PhC nanocavity switches [38,43]. However, as a high Q-factor can limit the operation speed, a smaller mode volume might be more favorable. For example, if the mode volume of the nanocavity is reduced by a factor of 20, which is feasible by employing the effect of extreme dielectric confinement [44], the generated pulse energy (0.85 fJ/pulse) will exceed the modulation energy (0.83 fJ/pulse), acting as an optical transistor. A more efficient modulation associated with a smaller mode volume could also help in narrowing the pulse width (Supplement 1 C.2).

In summary, we have experimentally demonstrated an ultrasmall cavity-dumped microscopic laser based on optical Fano resonance. By optically modulating the nanocavity-based Fano mirror, the laser generates optical pulses with peak power more than one order of magnitude higher than a corresponding gain-modulated FP laser. The cavity-dumping scheme relaxes the trade-off between the output peak power and modulating energy, an inherent issue for conventional gain-modulated lasers, and the small mode volume of the nanocavity helps reduce the energy consumption. Importantly, the laser cavity based on a Fano mirror sustains only a single lasing mode, essentially being a bound-state-in-the-continuum [35], ensuring that cavity dumping rather than mode switching is achieved. Our scheme based on optical Fano resonance can be extended to other configurations, including vertical [6] and hybrid integration [6,45], and can be combined with electrical modulation [46,47], which is essential for low-power, ultrafast chip-scale applications including conventional optical communication and computation [48–50], as well as spiking neuromorphic networks [51–53].

Funding. European Research Council (834410 FANO); Danmarks Grundforskningsfond (DNRF147 NanoPhoton); Villum Fonden via the NATEC Center (8692) and the Young Investigator Program (42026).

Acknowledgment. We thank M. Galili, M. Pu, and L.K. Oxenløwe for assistance with experimental equipment, and M. Xiong for inductively coupled plasma etching optimization and assistance with sample characterization.

Disclosures. The authors declare no competing interests.

Data availability. Data underlying the results presented in this paper may be obtained from the authors upon reasonable request.

Supplemental document. See Supplement 1 for supporting content.

REFERENCES

1. D. Miller, "Device requirements for optical interconnects to silicon chips," Proc. IEEE **97**, 1166–1185 (2009).
2. I. L. Markov, "Limits on fundamental limits to computation," Nature **512**, 147–154 (2014).
3. C. T. Phare, Y.-H. Daniel Lee, J. Cardenas, and M. Lipson, "Graphene electro-optic modulator with 30 GHz bandwidth," Nat. Photonics **9**, 511–514 (2015).
4. Q. Xu, B. Schmidt, S. Pradhan, and M. Lipson, "Micrometre-scale silicon electro-optic modulator," Nature **435**, 325–327 (2005).
5. B. Ellis, M. A. Mayer, G. Shambat, T. Sarmiento, J. Harris, E. E. Haller, and J. Vučković, "Ultralow-threshold electrically pumped quantum-dot photonic-crystal nanocavity laser," Nat. Photonics **5**, 297–300 (2011).
6. G. Crosnier, D. Sanchez, S. Bouchoule, P. Monnier, G. Beaudoin, I. Sagnes, R. Raj, and F. Raineri, "Hybrid indium phosphide-on-silicon nanolaser diode," Nat. Photonics **11**, 297–300 (2017).
7. H. Long, Y.-Z. Huang, Y.-D. Yang, L.-X. Zou, J.-L. Xiao, X.-W. Ma, X.-M. Lv, B.-W. Liu, and Y. Du, "High-speed direct-modulated unidirectional emission square microlasers," J. Lightwave Technol. **33**, 787–794 (2015).
8. X.-M. Lv, Y.-Z. Huang, L.-X. Zou, H. Long, and Y. Du, "Optimization of direct modulation rate for circular microlasers by adjusting mode Q factor," Laser Photon. Rev. **7**, 818–829 (2013).
9. L.-X. Zou, Y.-Z. Huang, X.-M. Lv, H. Long, J.-L. Xiao, Y.-D. Yang, and Y. Du, "Dynamic characteristics of AlGaInAs/InP octagonal resonator microlaser," Appl. Phys. B **117**, 453–458 (2014).
10. G. C. Park, W. Xue, M. Piels, D. Zibar, J. Mork, E. Semenova, and I. S. Chung, "Ultrahigh-speed Si-integrated on-chip laser with tailored dynamic characteristics," Sci. Rep. **6**, 38801 (2016).
11. K. Takeda, T. Sato, A. Shinya, K. Nozaki, W. Kobayashi, H. Taniyama, M. Notomi, K. Hasebe, T. Kakitsuka, and S. Matsuo, "Few-fJ/bit data transmissions using directly modulated lambda-scale embedded active region photonic-crystal lasers," Nat. Photonics **7**, 569–575 (2013).
12. S. Matsuo, A. Shinya, T. Kakitsuka, K. Nozaki, T. Segawa, T. Sato, Y. Kawaguchi, and M. Notomi, "High-speed ultracompact buried heterostructure photonic-crystal laser with 13 fJ of energy consumed per bit transmitted," Nat. Photonics **4**, 648–654 (2010).
13. H. Altug, D. Englund, and J. Vučković, "Ultrafast photonic crystal nanocavity laser," Nat. Phys. **2**, 484–488 (2006).
14. S. Matsuo and T. Kakitsuka, "Low-operating-energy directly modulated lasers for short-distance optical interconnects," Adv. Opt. Photon. **10**, 567 (2018).
15. W. R. Hook, R. H. Dishington, and R. P. Hilberg, "Laser cavity dumping using time variable reflection," Appl. Phys. Lett. **9**, 125–127 (1966).
16. J. Myers, C. Kokoczka, G. Cook, and R. Bedford, "High peak power cavity dumping semiconductor lasers," Opt. Lett. **42**, 113–116 (2017).
17. L. Harris, M. Clark, P. Veitch, and D. Ottaway, "Compact cavity-dumped Q-switched Er:YAG laser," Opt. Lett. **41**, 4309–4311 (2016).
18. S. Kaspar, M. Rattunde, T. Töpper, U. T. Schwarz, C. Manz, K. Köhler, and J. Wagner, "Electro-optically cavity dumped 2 μm semiconductor disk laser emitting 3 ns pulses of 30 W peak power," Appl. Phys. Lett. **101**, 141121 (2012).
19. V. G. Savitski, J. E. Hastie, S. Calvez, and M. D. Dawson, "Cavity-dumping of a semiconductor disk laser for the generation of wavelength-tunable micro-Joule nanosecond pulses," Opt. Express **18**, 11933–11941 (2010).
20. A. Killi, J. Dörring, U. Morgner, M. J. Lederer, J. Frei, and D. Kopf, "High speed electro-optical cavity dumping of mode-locked laser oscillators," Opt. Express **13**, 1916–1922 (2005).
21. A. Killi, U. Morgner, M. J. Lederer, and D. Kopf, "Diode-pumped femtosecond laser oscillator with cavity dumping," Opt. Lett. **29**, 1288–1290 (2004).
22. A. Baltuška, Z. Wei, M. S. Pshenichnikov, D. A. Wiersma, and R. Szipőcs, "All-solid-state cavity-dumped sub-5-fs laser," Appl. Phys. B **65**, 175–188 (1997).
23. G. N. Gibson, R. Klank, F. Gibson, and B. E. Bouma, "Electro-optically cavity-dumped ultrashort-pulse Ti:sapphire oscillator," Opt. Lett. **21**, 1055–1057 (1996).
24. P. Dong, A. Melikyan, K. Kim, N. Kaneda, B. Stern, and Y. Baeyens, "In-phase/quadrature modulation using directly reflectivity-modulated laser," Optica **7**, 929–933 (2020).
25. P. Dong, A. Maho, R. Brenot, Y. Chen, and A. Melikyan, "Directly reflectivity modulated laser," J. Lightwave Technol. **36**, 1255–1261 (2018).
26. V. Shchukin, N. Ledentsov, J. Lott, H. Quast, F. Hopfer, L. Y. Karachinsky, M. Kuntz, P. Moser, A. Mutig, A. Strittmatter, V. Kalosha, and D. Bimberg, "Ultra high-speed electro-optically modulated VCSELs: modeling and experimental results," Proc. SPIE **6889**, 98–112 (2008).
27. N. Tessler, M. Margalit, G. Eisenstein, and U. Koren, "Wide-band amplitude modulation by electrooptic tuning of the center wavelength in short-cavity distributed Bragg reflector lasers," IEEE J. Sel. Top. Quantum Electron. **1**, 490–493 (1995).

28. S. Fan, "Sharp asymmetric line shapes in side-coupled waveguide-cavity systems," Appl. Phys. Lett. **80**, 908–910 (2002).
29. U. Fano, "Effects of configuration interaction on intensities and phase shifts," Phys. Rev. **124**, 1866–1878 (1961).
30. M. F. Limonov, M. V. Rybin, A. N. Poddubny, and Y. S. Kivshar, "Fano resonances in photonics," Nat. Photonics **11**, 543–554 (2017).
31. B. Luk'yanchuk, N. I. Zheludev, S. A. Maier, N. J. Halas, P. Nordlander, H. Giessen, and C. T. Chong, "The Fano resonance in plasmonic nanostructures and metamaterials," Nat. Mater. **9**, 707–715 (2010).
32. Y. Yu, W. Xue, E. Semenova, K. Yvind, and J. Mork, "Demonstration of a self-pulsing photonic crystal Fano laser," Nat. Photonics **11**, 81–84 (2017).
33. J. Mork, Y. Chen, and M. Heuck, "Photonic crystal Fano laser: terahertz modulation and ultrashort pulse generation," Phys. Rev. Lett. **113**, 163901 (2014).
34. T. S. Rasmussen, Y. Yu, and J. Mork, "Suppression of coherence collapse in semiconductor Fano lasers," Phys. Rev. Lett. **123**, 233904 (2019).
35. Y. Yu, A. Sakanas, A. R. Zali, E. Semenova, K. Yvind, and J. Mørk, "Ultra-coherent Fano laser based on a bound state in the continuum," Nat. Photonics **15**, 758–764 (2021).
36. K. Y. Lau, "Gain switching of semiconductor injection lasers," Appl. Phys. Lett. **52**, 257–259 (1988).
37. A. Faraon, I. Fushman, D. Englund, N. Stoltz, P. Petroff, and J. Vučković, "Dipole induced transparency in waveguide coupled photonic crystal cavities," Opt. Express **16**, 12154–12162 (2008).
38. Y. Yu, E. Palushani, M. Heuck, N. Kuznetsova, P. T. Kristensen, S. Ek, D. Vukovic, C. Peucheret, L. K. Oxenløwe, S. Combrié, A. de Rossi, K. Yvind, and J. Mørk, "Switching characteristics of an InP photonic crystal nanocavity: Experiment and theory," Opt. Express **21**, 31047–31061 (2013).
39. S. Yan, H. Chen, S. Gao, F. Zhou, S. Xiao, Y. Ding, J. Dong, X. Cai, and X. Zhang, "Efficient thermal tuning employing metallic microheater with slow-light effect," IEEE Photon. Technol. Lett. **30**, 1151–1154 (2018).
40. L. D. Haret, X. Checoury, F. Bayle, N. Cazier, P. Boucaud, S. Combrie, and A. de Rossi, "Schottky MSM junctions for carrier depletion in silicon photonic crystal microcavities," Opt. Express **21**, 10324–10334 (2013).
41. V. Eckhouse, I. Cestier, G. Eisenstein, S. Combrié, G. Lehoucq, and A. De Rossi, "Kerr-induced all-optical switching in a GaInP photonic crystal Fabry-Perot resonator," Opt. Express **20**, 8524–8534 (2012).
42. M. Li, J. Ling, Y. He, U. A. Javid, S. Xue, and Q. Lin, "Lithium niobate photonic-crystal electro-optic modulator," Nat. Commun. **11**, 4123 (2020).
43. K. Nozaki, T. Tanabe, A. Shinya, S. Matsuo, T. Sato, H. Taniyama, and M. Notomi, "Sub-femtojoule all-optical switching using a photonic-crystal nanocavity," Nat. Photonics **4**, 477–483 (2010).
44. M. Albrechtsen, B. Vosoughi Lahijani, R. E. Christiansen, V. T. H. Nguyen, L. N. Casses, S. E. Hansen, N. Stenger, O. Sigmund, H. Jansen, J. Mork, and S. Stobbe, "Nanometer-scale photon confinement in topology-optimized dielectric cavities," Nat. Commun. **13**, 6281 (2022).
45. M. D. Birowosuto, A. Yokoo, G. Zhang, K. Tateno, E. Kuramochi, H. Taniyama, M. Takiguchi, and M. Notomi, "Movable high-Q nanoresonators realized by semiconductor nanowires on a Si photonic crystal platform," Nat. Mater. **13**, 279–285 (2014).
46. K. Nozaki, S. Matsuo, T. Fujii, K. Takeda, A. Shinya, E. Kuramochi, and M. Notomi, "Femtofarad optoelectronic integration demonstrating energy-saving signal conversion and nonlinear functions," Nat. Photonics **13**, 454–459 (2019).
47. E. Dimopoulos, A. Sakanas, A. Marchevsky, M. Xiong, Y. Yu, E. Semenova, J. Mørk, and K. Yvind, "Electrically-driven photonic crystal lasers with ultra-low threshold," Laser Photon. Rev. **16**, 2200109 (2022).
48. A. H. Atabaki, S. Moazeni, F. Pavanello, H. Gevorgyan, J. Notaros, L. Alloatti, M. T. Wade, C. Sun, S. A. Kruger, H. Meng, K. Al Qubaisi, I. Wang, B. Zhang, A. Khilo, C. V. Baiocco, M. A. Popovic, V. M. Stojanovic, and R. J. Ram, "Integrating photonics with silicon nanoelectronics for the next generation of systems on a chip," Nature **556**, 349–354 (2018).
49. C. Sun, M. T. Wade, Y. Lee, *et al.*, "Single-chip microprocessor that communicates directly using light," Nature **528**, 534–538 (2015).
50. H. J. Caulfield and S. Dolev, "Why future supercomputing requires optics," Nat. Photonics **4**, 261–263 (2010).
51. J. Feldmann, N. Youngblood, C. D. Wright, H. Bhaskaran, and W. H. P. Pernice, "All-optical spiking neurosynaptic networks with self-learning capabilities," Nature **569**, 208–214 (2019).
52. M. Miscuglio, G. C. Adam, D. Kuzum, and V. J. Sorger, "Roadmap on material-function mapping for photonic-electronic hybrid neural networks," APL Mater. **7**, 100903 (2019).
53. B. J. Shastri, A. N. Tait, T. Ferreira de Lima, W. H. P. Pernice, H. Bhaskaran, C. D. Wright, and P. R. Prucnal, "Photonics for artificial intelligence and neuromorphic computing," Nat. Photonics **15**, 102–114 (2021).